

On the Collision of Sea Breeze Gravity Currents

Karin van der Wiel

September 30, 2013

1 Introduction

The diurnal cycle of solar heating often generates sea and land breezes in coastal regions. Differences in heating over land and sea create horizontal density differences that set up the sea/land breeze front. The horizontal extent of these circulations have been shown to depend strongly on latitude [12, 22, 1]. In England (50°N) sea breeze fronts have been observed 100 km inland [20]; in southern Australia (32°S) fronts travel as far as 400 km [6].

The large horizontal extent implies that for narrow peninsulas, islands or seas, converging sea breezes from opposing shorelines can meet. Horizontal convergence of sea breezes may be responsible for direct initiation of deep convection [4]. Examples of this include, southern Florida where the convergence of sea breezes is one of the dominating controls of the location of thunderstorm complexes [3, 15]; the Cape York Peninsula (Australia) where the North Australian Cloud Line is linked to double sea breezes [13]; and the Hector thunderstorms over the Tiwi Islands (Australia) which get part of their convective strength from the convergence generated by two nearby coastlines [4, 8]. Over bodies of water not wider than 500 km convergence of two land breezes can be expected [10, 9].

Converging sea breezes have been studied using observational data and numerical simulations. These studies have focused on different aspects of the collision. For example, vertical velocities were found to be maximum if the sea breezes were to collide between 14:00 and 17:00 local time [21], given a sea breeze propagation rate across an island the optimal width of the island resulting in maximum vertical velocities can thus be computed. The sea breeze fronts that collided before or after this time window were slightly weaker and therefore generated weaker vertical motions in the numerical simulations performed in [21]. The height of the sea breeze front is influenced by both the direction of the surface wind and the direction of low-level shear. Depending on whether those point in the same direction the effects on meeting currents can be one of two: either the gravity current height remains unchanged on both shores or at one shore the height might be enhanced while it is being suppressed at the other shore, increasing the height difference during collision [11]. Finally, [7] discusses the formation of atmospheric undular bores by the rising of cool, moist sea breeze air into a warmer environment.

Sea breeze fronts are one practical example of gravity currents. Gravity currents, sometimes referred to as density or buoyancy currents, are flows driven by horizontal density differences. The study of converging gravity currents is also relevant in situations other than sea breezes. Another example of meteorological gravity currents are the cold downdrafts from thunderstorms, these are fronts of cold air that can interact with other downdraft fronts

or other pre-existing fronts. Other natural examples of gravity currents include the spreading of oil slicks in the ocean, avalanches and volcanic pyroclastic flows [18]. In industry gravity currents provide a description of the spreading of dense gases into the environment [16]. In the unfortunate case of an accident it is important to have accurate predictions of the spreading and any interactions that might follow.

In the laboratory, ‘lock-exchange’ experiments can be used to create gravity currents. Few experimental studies of colliding gravity currents have been published. A lab experiment discussed in [18, p. 196-197] shows the emergence of two bores traveling in opposite directions. This result was confirmed in a numerical simulation [14]. A more extensive discussion of colliding gravity currents can be found in [16], which presents experimental results based on collisions of currents of equal density but different heights. The study also develops a global theory for the propagation speed of the incoming gravity currents and resulting bores based on momentum and energy conservation.

Before the collision takes place, there are two horizontal propagating gravity currents. After the lock-release there is a short period of acceleration, after which the current enters the constant-speed regime. There exist multiple theories of what this speed should be and all are based on the non-dimensional Froude number:

$$U_1 = F_H \sqrt{g'_1 H_1}, \quad (1)$$

where U_1 is the propagation speed, F_H is a dimensionless Froude number, g'_1 is the reduced gravity and H_1 is the lock height [18]. The reduced gravity is based on the density difference between the gravity current (ρ_1) and the ambient fluid (ρ_0):

$$g'_1 = \frac{\rho_1 - \rho_0}{\rho_1} g. \quad (2)$$

Different authors have presented different theories for what the Froude number should be. In this study the Froude number as defined in [17] will be used throughout:

$$F_H = \frac{\sqrt{2 - H_1/H_0}}{2}, \quad (3)$$

with H_0 the total depth of the fluid.

The objective of this study is to investigate what happens during the collision of two sea breeze fronts. Laboratory experiments of two colliding gravity currents in a rectangular channel are presented. These experiments have been designed to test the influence of differences in density, height and speed of two meeting gravity currents on the collision. In the remainder of this report different aspects of these collisions are discussed. Section 2 gives a description of the experimental setup and the experiments performed. Experimental results are presented in Section 3, some theoretical consideration is mentioned in Section 4. A final discussion is given in Section 5.

2 Experimental setup

All experiments were carried out in a horizontal rectangular channel. The tank used in this study was made of glass, 150 cm long and 15.5 cm deep. In all cases the tank was filled to

a depth of $H_0 = 20$ cm. The tank was lit from the back using a light sheet that was the same size as the back wall of the tank. Experiments were filmed using a video camera at approximately 2 m distance.

At both ends of the tank a separate section, a ‘lock’, was made using a vertical barrier, the ‘lock gate’. The locks were 20 cm long. In the locks salt (NaCl) was added to the water to increase the density and thus create the horizontal density differences needed for the gravity currents. Yellow and blue food dye was added to distinguish the denser fluids from the transparent, fresh, ambient fluid after lock release. Densities were measured using a density meter with a precision of 10^{-4} g cm $^{-3}$. A schematic of the experimental setup is shown in Figure 1.

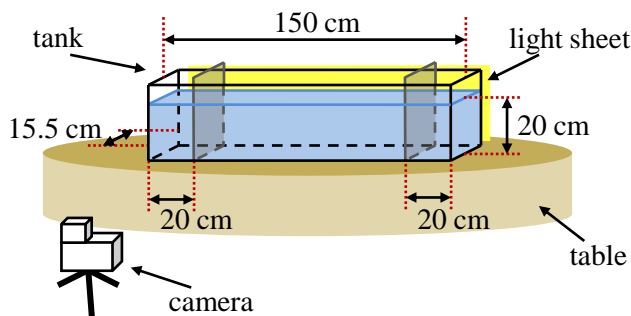


Figure 1: Experimental setup.

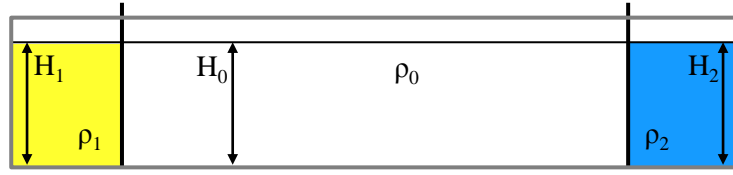
Two sets of experiments were performed. The first set was designed to study the influence of (relative) differences in reduced gravity on the collision. This set of experiments will be referred to as ‘full-depth’ lock exchanges or ‘full-depth’ experiments. Both locks were filled to the top with dense fluid, i.e. $H_1 = H_2 = H_0$ (Figure 2a), where H_0 is the total depth of the fluid and H_1 and H_2 are the height of denser fluid in the two locks. In total eighteen experiments were done; these are mapped out in parameter space in the lower panels of Figure 2. The ratio of the reduced gravities ranged from $0.22 < r_g < 0.99$, where r_g is defined as

$$r_g = \frac{g'_{light}}{g'_{heavy}}. \quad (4)$$

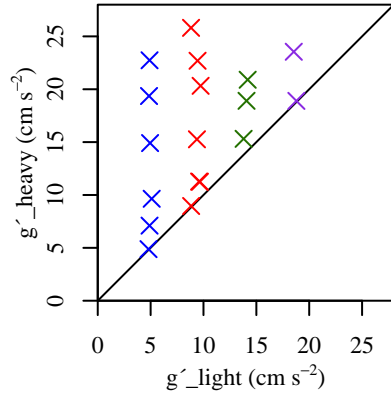
In the second set of experiments the depth of one of the locks was half of the total depth ($H_1 = H_0$, $H_2 = \frac{1}{2}H_0$, Figure 3a). A second independent parameter, gravity current height, has been introduced to the problem this way. These experiments are a more realistic representation of the environmental sea breeze convergence, as for those both the density and height of the meeting fronts might be different. In total fourteen half-depth experiments were done.

Finally, four additional partial-depth experiments were done for different ratios of the lock height. The $g'_1 H_1$ and $g'_2 H_2$ values for the meeting gravity currents were kept constant at approximately 100 cm 2 s $^{-2}$, but different combinations of g' and H were used. An overview of the initial conditions of all experiments is given in Appendix A.

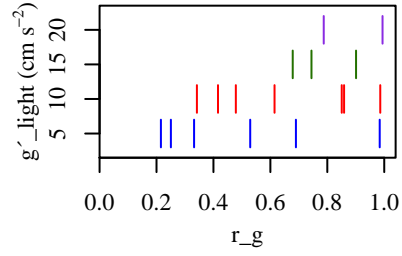
At the start of the experiments the lock gates were pulled up vertically. There was always a short period of acceleration, but soon after the release the gravity currents entered



(a)

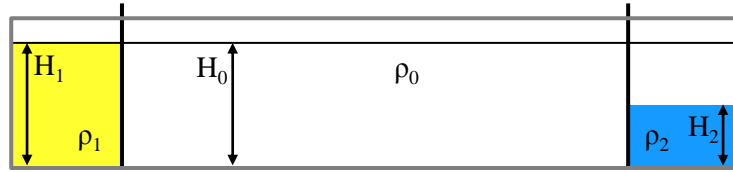


(b)

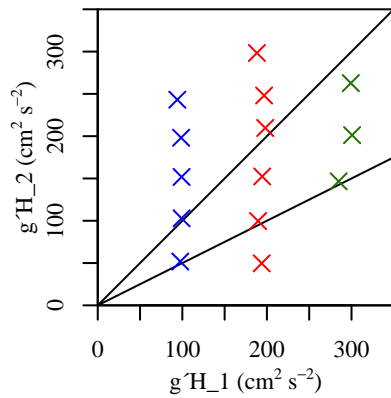


(c)

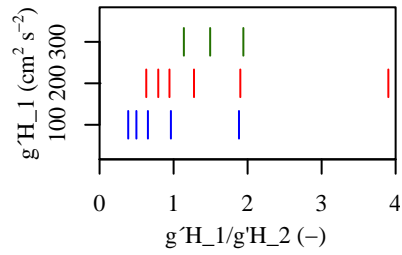
Figure 2: (a) Schematic of the initial setup for the full-depth experiments. (b,c) Position in parameter space of all full-depth experiments performed.



(a)



(b)



(c)

Figure 3: (a) Schematic of the initial setup for the half-depth experiments. (b,c) Position in parameter space of all half-depth experiments performed.

the constant-speed regime. The collision event always happened within this regime. Viscous effects do not play a role as the Reynolds numbers based on gravity current height (h) and speed (U),

$$Re = \frac{Uh}{\nu}, \quad (5)$$

was always above 3500, well above the critical value of a 1000 [18, p.141]. At the end of most experiments water samples from different depths in the tank were analyzed using the density meter to create a density profile. In the bottom half of the tank two samples were taken every centimeter water depth, in the top half every five centimeters. These data were then used to compute mixing efficiency data.

3 Experimental results

Snapshots from two full-depth experiments are shown in Figure 4. The left column shows a symmetric case, where g'_1 was equal to g'_2 ($r_g = 0.99$); the right column is an asymmetric case with heavier blue fluid ($r_g = 0.33$).

Different aspects of these experiments will be discussed in this section of the report. In Section 3.1 the propagation speed of the gravity currents before collision (Figures 4a and 4b) will be discussed and compared to the theoretical predictions. The collision will be analyzed in more detail in Section 3.2, which considers both the initial collision angle

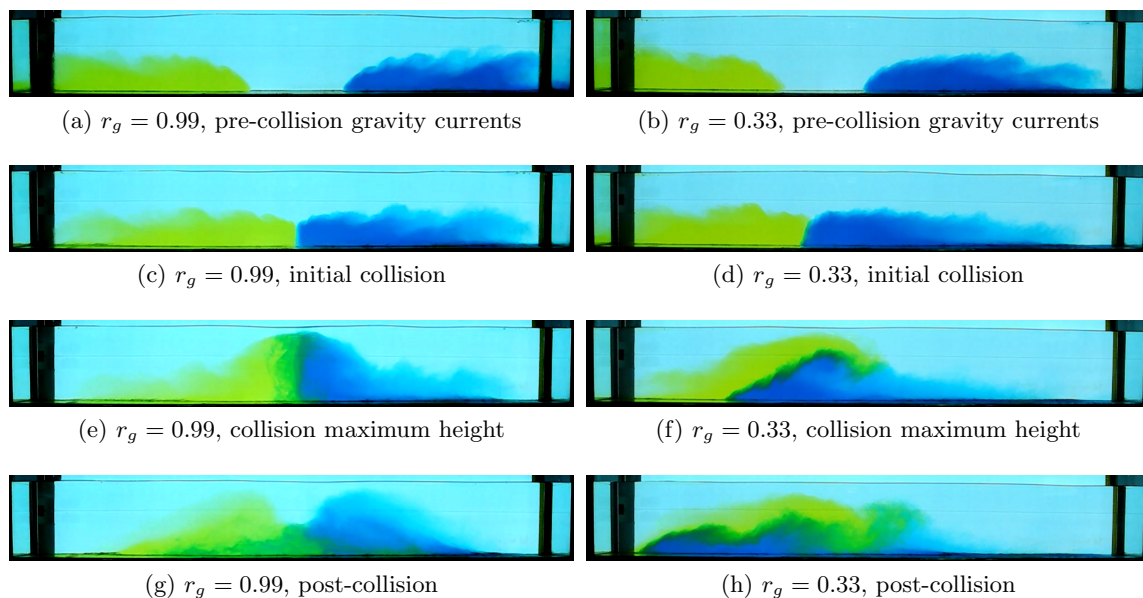


Figure 4: Snapshots of two experiments at different times. Note that the time difference between different panels is not the same for the two experiments. Times shown: (a,b) pre-collision gravity currents, (c,d) initial collision, (e,f) collision maximum height, (g,h) post-collision. Experiments shown: (a,c,e,g) symmetric case with $r_g = 0.99$, (b,d,f,h) asymmetric case with $r_g = 0.33$.

(Figures 4c and 4d) and the maximum height (Figures 4e and 4f). Last, total mixing in the tank will be discussed in Section 3.3.

3.1 Pre-collision gravity currents

Figure 5 compares measured propagation speeds and Froude numbers of the experimental gravity currents with theoretical prediction using Equations 1 and 3. For clarity only currents from full-depth (53 currents) and half-depth (16 currents) locks are shown. Theoretical curves are plotted for both lock heights. Lower lock heights create slower propagating gravity currents with a higher Froude number. For all currents except one, the measured speeds are lower than the theory predicts. This can be explained by assumptions made in the derivation of the equations. The theory assumes no energy loss due to friction, mixing or viscosity. The Reynolds numbers in the experiments were sufficiently high to meet the last criterion, but effects from friction and mixing cannot be neglected.

Froude numbers are about 15% lower than the theoretical value, independent of the value of g' or the height H_1 of fluid in the lock. For the full-depth experiments we find a mean Froude number of 0.42 instead of the 0.5 from theory. The mean Froude number for the half-depth lock experiments is 0.53, where theory predicted 0.61. These values are slightly lower than the Froude numbers found in [17], these were 0.46 ± 0.015 and 0.57 ± 0.015 for full-depth and half-depth lock exchanges respectively.

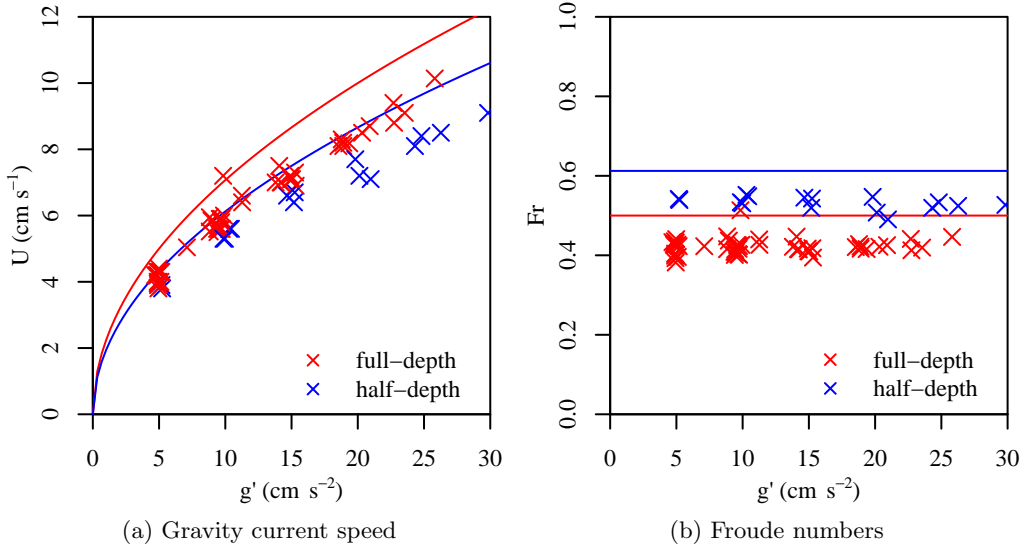


Figure 5: (a) Gravity current propagation speed versus reduced gravity. (b) Froude numbers versus reduced gravity. In both panels the marks are all individual experiments, lines are the theoretical values based on Equations 1 and 3. The red marks and line correspond to the full-depth lock experiments, blue symbols mark the half-depth experiments.

3.2 Collision

Figure 6 shows the first second of a collision event in more detail. Frames from the experimental videos were analyzed to find the position of the fronts in time. Both sequences start at time = 0, which is the first frame at which the fronts collide. The next frames are 5 frames ≈ 165 ms apart, up to frame 30 ≈ 1 s after first collision. The plots show a short period spanning around what was shown in Figures 4c and 4d.

In the symmetric case of equal g' (Figure 6a) the shape of the fronts is similar and the collision front is vertical. In time this front extends in height and remains vertical, and mixing occurs on the front line. This can also be seen in Figures 4c and 4e. The asymmetric case is different (Figure 6b). Before colliding, the fronts are already changing shape and therefore have different steepness upon collision. The collision front develops at an angle with the heavier fluid (blue) pushing underneath the lighter fluid. The front shape is not steady in time, after a while (in this case half a second, 15 frames) a new gravity current forms at the bottom and Kelvin-Helmholtz billows develop at the top. The front transforms from an initial straight line at an angle to an ‘S’ shaped front that changes shape to being more horizontal in time.

The initial angle changes for different experiments. This angle is defined as the angle θ between the front and the vertical, positive clockwise with denser fluid to the right. To clarify, in Figures 4c and 6a this angle is 0° , in Figures 4d and 6b (frames 5 and 10) the angle is about 16° . The initial collision angles for all experiments performed are plotted in Figure 7 against r_g . The three colours mark the different sets of experiments. However

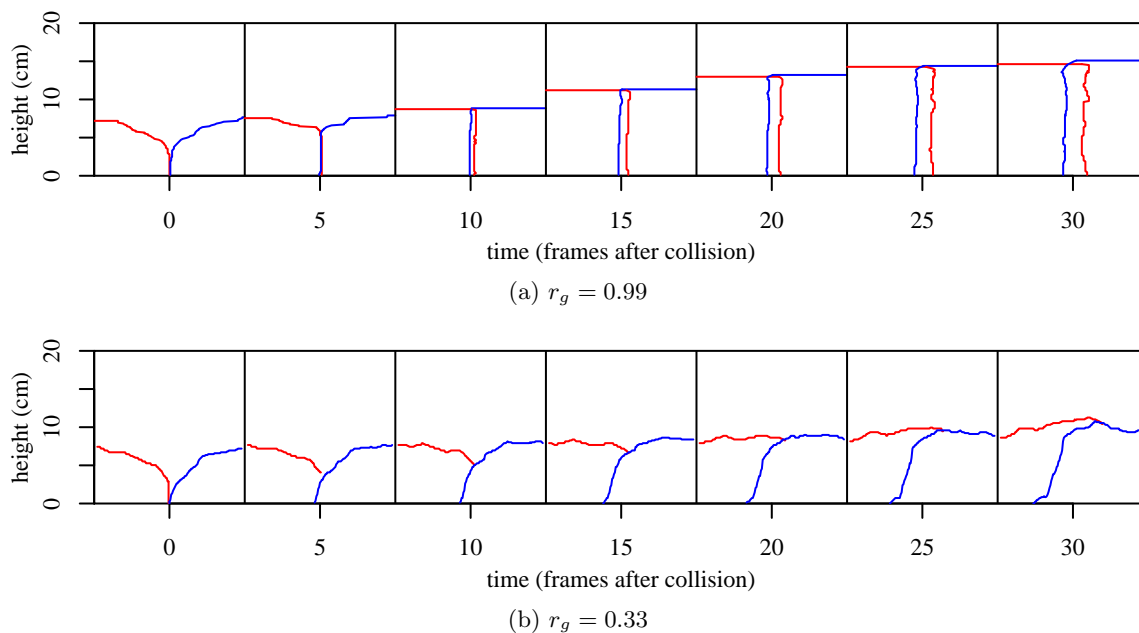


Figure 6: Analyzed front positions at and after collision for two different experiments. Along the horizontal different time frames in the experimental videos are shown, one frame corresponds to 33 ms. Experiments shown: (a) $r_g = 0.99$ (b) $r_g = 0.33$, these are the same experiments as shown in Figure 4.

the data are not clustered by these sets, and the height of the incoming gravity currents seems not to affect the initial collision angle. The relation between the collision angle and the ratio of g' , r_g , is clear from the data. For near-symmetric experiments ($r_g \approx 1.0$) the angle is small and the collision front is almost vertical. For increasingly asymmetric cases the front tilts, with the heavier fluid sitting underneath the lighter fluid. The collision angle increases from 0° for $r_g = 1.0$ to about 20° for $r_g = 0.2$. The slope of the linear regression line is $-25.53 \pm 2.55^\circ$.

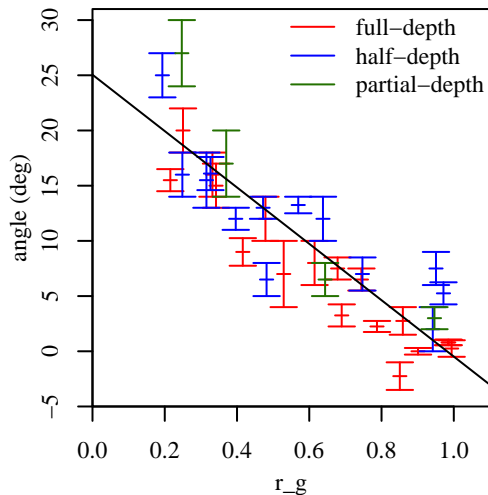


Figure 7: Initial collision angle set against ratio r_g . The red marks correspond to the full-depth lock experiments, blue marks correspond to the half-depth experiments, green marks are the final four partial-depth experiments. The black line is the linear fit to all data.

In addition to the angle of the collision front, temporal changes in the height of the front are also of interest. The heights of the moving gravity currents and the maximum height of the colored fluid were measured in each experiment. For the full-depth lock releases, energy-conservation theory predicts that the height of the gravity current is half the total water depth [2]. The full-depth lock release gravity currents presented here have a similar value (see Figure 8). In the full-depth experiments, Figure 8a, the maximum height after collision is approximately 0.90 of the total water depth independent of r_g . This height is not reached after a constant time difference after the collision event, as can be seen in Figure 6. The colored fluid in the experiment shown in Figure 6a reaches 15 cm after one second (frame 30), in the asymmetric case it only goes up to 11 cm after the first second. Preliminary analysis on the speed of this rise seems to point to a dependence on the propagation speeds of the incoming gravity currents. However it is difficult to quantify the exact vertical speed from the current experimental setup. The half-depth experiments (coloured marks in Figure 8b) show more variation in collision height with r_g , though the spread is large.

In the partial-depth experiments (black in Figure 8b) we have a symmetric case of two half-depth locks ($r_g \approx 1.0$). The maximum height reached in this experiment was 0.75 of the total water depth, higher than the initial lock heights. Based on this result, a hypothesis can

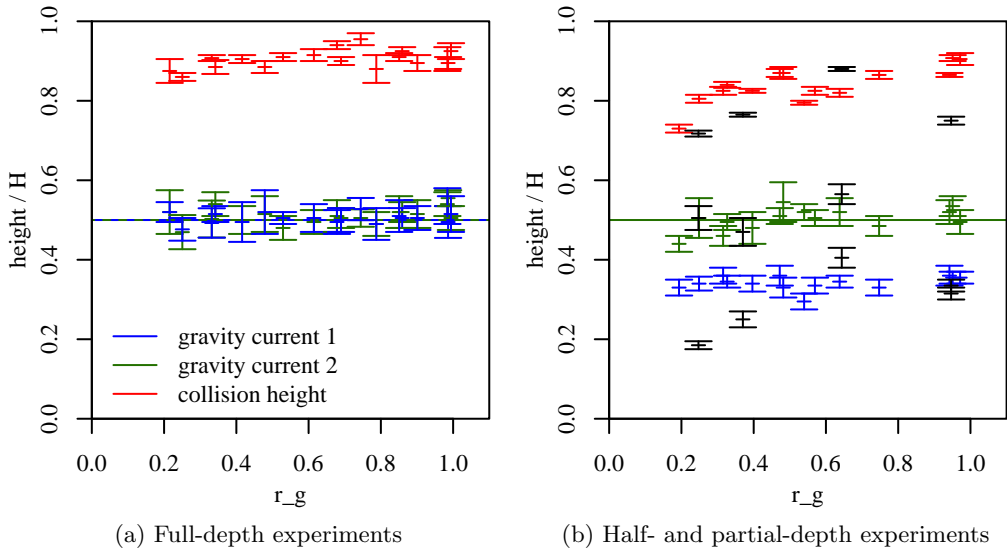


Figure 8: Pre-collision gravity current heights and maximum height reached after collision against ratio r_g . All heights are normalized by the total water depth, H_0 . The horizontal lines show the theoretical, energy conserving value for the height of a gravity current from a full-depth lock. (a) Full-depth experiments, (b) half-depth experiments in the same colours as (a) and partial-depth experiments in black.

be formed that different processes near the water surface (at H_0) might have influenced or ultimately stopped the rise of colored fluid in the full-depth experiments. Motivated by the different results of the collision of two symmetric currents from full-depth lock-exchanges and the collision of two currents from symmetric half-depth experiments.

3.3 Post-collision mixing

As a measure of mixing in the tank we use mixing efficiency. This is defined as fraction of energy lost from the total Potential Energy (PE) during the experiment:

$$E_M = 1 - \frac{PE_{t=0} - PE_{profile}}{PE_{t=0} - PE_{rearranged}}, \quad (6)$$

where $PE_{t=0}$ is the potential energy in the initial set up before lock release, $PE_{profile}$ the potential energy in the measured density profile at the end of the experiments and $PE_{rearranged}$ is the minimum potential energy in the theoretical case of no mixing. This rearranged profile is therefore the densest fluid at the bottom and lightest fluid on top, in a stepfunction like profile. PE is computed through:

$$PE = \int_0^{H_0} \rho g z \, dz. \quad (7)$$

The mixing data for the full-depth experiments is plotted against the mean Reynolds number in Figure 9a. The mean Reynolds number is the geometric mean of the Reynolds

numbers of the two incoming gravity currents before collision (Equation 5). There is enhanced energy loss due to mixing with increasing Reynolds number. This was also found in previous experiments [5]. No relationship was found with r_g . The mixing data of the half-depth lock experiments do not exhibit this relation with Reynolds number (Figure 9a).

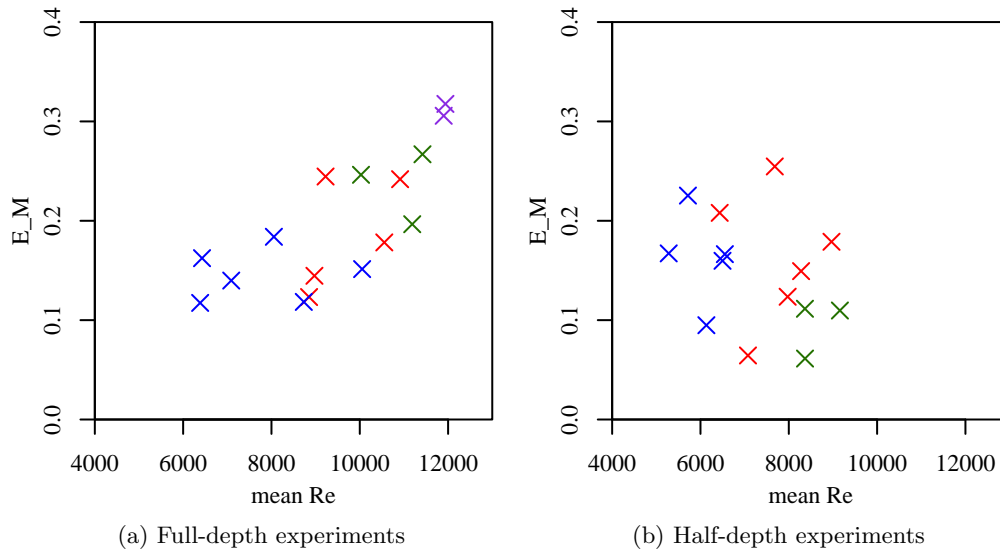


Figure 9: Mixing efficiency against mean Reynolds number of the two incoming gravity currents. (a) Full-depth experiments, (b) half-depth experiments. Colors as in Figures 2b and 3b.

4 Theoretical considerations

Two different models will be presented as an attempt to predict the initial collision angle based on knowledge of two incoming asymmetrical gravity currents. The first model is a steady state model, based on conservation of mass and horizontal momentum. It has some similarities with existing theories for colliding jets. The second model is not steady and is based on the generation of a shear flow from horizontal density gradients [19].

4.1 Momentum conservation

Consider two gravity currents (ρ_1, U_1, h_1 and ρ_2, U_2, h_2) propagating towards each other and colliding at stagnation point O . At collision the two fluids rise under angle θ to a height D . The ambient fluid has density ρ_0 and height H_0 , atmospheric pressure at the top is considered to be zero. Figure 10 shows a schematic of this flow.

We will consider the angle in a frame of reference where the stagnation point is at rest. Hence:

$$U_1 - \Delta U = U_2 + \Delta U = U_{in}. \quad (8)$$

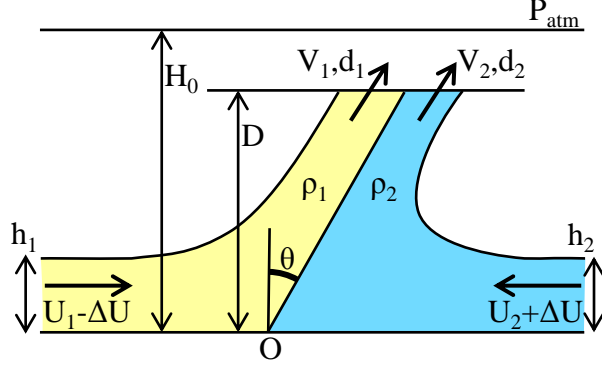


Figure 10: Schematic of collision in a frame of reference where the stagnation point O is at rest.

Rearranging, we find for the incoming gravity current speeds:

$$U_{in} = \frac{U_1 + U_2}{2} \quad (9)$$

and

$$\Delta U = \frac{U_1 - U_2}{2}. \quad (10)$$

Mass conservation for the two fluids gives:

$$h_1 U_{in} = d_1 V_1 \cos \theta, \quad (11)$$

$$h_2 U_{in} = d_2 V_2 \cos \theta. \quad (12)$$

Conservation of horizontal momentum gives:

$$\begin{aligned} -\rho_1 U_{in}^2 h_1 - \frac{1}{2} \rho_1 g'_1 h_1^2 + \rho_2 U_{in}^2 h_2 + \frac{1}{2} \rho_2 g'_2 h_2^2 \\ + \rho_1 V_1^2 d_1 \sin \theta \cos \theta + \rho_2 V_2^2 d_2 \sin \theta \cos \theta = 0. \end{aligned} \quad (13)$$

Rearranging this momentum equation and using Equations 11 and 12 to replace the $d \cos \theta$ terms, we find for the angle θ :

$$\sin \theta = \frac{U_{in}^2 (\rho_2 h_2 - \rho_1 h_1) + \frac{1}{2} (\rho_2 g'_2 h_2^2 - \rho_1 g'_1 h_1^2)}{-\rho_1 V_1 U_{in} h_1 - \rho_2 V_2 U_{in} h_2}. \quad (14)$$

This is not a closed system, as the speeds V_1 and V_2 are unknown. One could use steady Bernoulli along the streamlines at the top of the gravity current to find these, but that would introduce the unknown height D to the problem.

Instead the magnitude and sign of the incoming momentum fluxes will be considered in relation to the angle. In equation 14 the denominator is always negative, therefore any changes in sign of θ must originate from the relative magnitudes of the two incoming horizontal momentum terms. Using theoretical predictions for speed and height of gravity

currents from full-depth lock releases [2, 17] we can rewrite the numerator of Equation 14 to:

$$\frac{1}{16} \left(\sqrt{g'_1 H_0} + \sqrt{g'_2 H_0} \right)^2 (\rho_2 - \rho_1) + \frac{1}{4} (\rho_2 g'_2 - \rho_1 g'_1) H_0. \quad (15)$$

For a case where $\rho_2 > \rho_1$, i.e. heavier fluid to the right, this will result in $\sin \theta < 0$ and thus $\theta < 0$. The heavier fluid pushes over the lighter fluid. All experiments have resulted in the opposite scenario, with the heavier fluid going underneath the lighter fluid: so that for $\rho_2 > \rho_1$ the measured angle θ was always positive. It can therefore be concluded that the assumptions made in the derivation of this model are incorrect. These assumptions include hydrostatic pressure everywhere in the ambient fluid, the unknown time-varying collision height D and the steady-state framework. The collision angle is not stationary in time. Close analysis of the experimental videos points towards the existence of an initial collision angle that, as time goes on, increases, i.e. rotates towards the horizontal. A steady approximation as presented here is thus not applicable.

4.2 Shear flow

Fluids with horizontal density gradients in the presence of a vertical gravitational field are known to generate a horizontal flow with vertical shear. In the experiments presented here these gradients are always present, e.g. the horizontal density gradient associated with a gravity current propagating through an ambient fluid or, after collision, the horizontal density gradient between the two fluids from the locks.

The shape of the generated horizontal shear flow can be derived in the case of a constant density gradient as shown in [19]. For an initial density profile with a constant gradient α in the horizontal direction x and gradient β in the vertical, z .

$$\rho_0 = \bar{\rho}(1 - \alpha x - \beta z), \quad (16)$$

it is found that

$$u = g\alpha zt \quad (17)$$

and

$$\rho = \rho_0 - \frac{1}{2} g\bar{\rho}\alpha^2 zt^2. \quad (18)$$

The generated flow is sheared in the vertical and accelerates linearly in time. The horizontal density gradient remains constant, the vertical stratification increases in strength. The isopycnals therefore rotate towards the horizontal,

$$\tan \theta = \frac{\beta}{\alpha} + \frac{1}{2} g\alpha t^2. \quad (19)$$

When this model is applied to the collision experiments the change in the angle is too fast. Even though it is difficult to determine precisely, the evolution of $\tan(\theta)$ and ρ seems to be more linear than quadratic. Of course the assumption of a constant linear density gradient is poor, and a continuous gradient or a piecewise gradient description would fit better. In that case the generated flow will not be constant in the horizontal, and frontogenesis will take place. An in depth analysis of these situations is beyond the scope of the work during the GFD summer.

5 Discussion

Laboratory experiments for sea breeze collision have been performed and presented. Two gravity currents from a lock-release were made to collide in a rectangular tank. Both the density of the currents and the height of the currents were varied in the different experiments, which allowed for an analysis of the influence of density differences, height differences and horizontal propagation speed difference on the collision. The main conclusions are as follows.

(i) Before collision and far apart, the gravity currents speeds match the existing theory well and propagate with a Froude number about 15% lower than energy conserving theory predicts [17].

(ii) At collision a sharp front between the two fluids develops. The angle of the front with the vertical is dependent on the ratio between the two densities (r_g) only, and no relation was found with ratios of current heights or propagation speeds. For a collision of two symmetrical currents ($r_g = 1.0$) the front is vertical. The angle of the front increases linearly with increasing density difference, up to about 20° for $r_g = 0.2$. Attempts to predict the angle of the front using horizontal momentum arguments or generated shear flows were unsatisfactory.

(iii) No conclusions can be drawn on the maximum height reached by the colored fluids during collision. The full-depth lock experiments gave different results than the half-depth and partial-depth experiments.

(iv) For colliding gravity currents of equal height energy losses due to mixing are enhanced with increasing Reynolds number, in agreement with previous experiments [5]. For meeting currents of different height no relationship was found.

In the natural environment sea breeze currents are influenced by many different factors. Over islands and peninsulas, their collisions are therefore complex. The experiments in this report were designed to give a physical description of such collisions, which are very difficult to measure in detail in nature. The initial angle of the front is the line along which moist air parcels will rise from the sea breeze into drier ambient air. Condensation of water vapor will set off heavy cloud formation and if strong enough create thunderstorms. For nearly vertical fronts all this energy and the related rainfall will be concentrated over a very small surface area, whereas in the case of a tilted front this will be spread over a much larger surface area. The precipitation rate might therefore be partly dependent on the tilt of the front. In the experiments the angle of the front was set by the difference in density. Coasts with very different land use or seas with different temperatures could generate different heating rates and thus sea breeze gravity currents with different densities. In more symmetrical configurations of peninsulas and seas one would therefore expect currents of more equal density.

Predicting the angle of the collision front and its horizontal speed are of large scientific importance. The experiments presented in this report give an initial description of the collision, but attempts to create a model to predict the tilt have not been successful so far. More information of the exact flow patterns in the gravity currents, the ambient fluid and at the collision event would be very valuable. This information could be obtained by performing similar experiments but with the added technology of particle image velocimetry. Another option would be to set up numerical experiments and model the collision event.

Both methods would provide a detailed description of the horizontal and vertical flow before, at and after the collision of two gravity currents.

Acknowledgements

Many thanks to Sarah Gille, Stefan Llewellyn Smith, Claudia Cenedese and Paul Linden, who were all involved in this project and offered great advice throughout the summer. Thanks also to Anders Jensen and Bruce Sutherland for their practical help in the laboratory. The experiments were not possible without someone helping me out, so thanks to Catherine, Kate, Barbara, Luisa and many others for lifting the second lock. Finally, all the fellows, what a great summer we had. We got it. Somehow.

References

- [1] R W ARRITT, *Numerical modelling of the offshore extent of sea breezes*, Quarterly Journal of the Royal Meteorological Society, 115 (1989), pp. 547–570.
- [2] T B BENJAMIN, *Gravity currents and related phenomena*, Journal of Fluid Mechanics, 31 (1968), pp. 209–248.
- [3] H R BYERS AND H R RODEBUSH, *Causes of thunderstorms of the Florida peninsula*, Journal of Meteorology, 5 (1948), pp. 275–280.
- [4] R E CARBONE, J W WILSON, T D KEENAN, AND J M HACKER, *Tropical island convection in the absence of significant topography. Part I: Life cycle of diurnally forced convection*, Monthly Weather Review, 128 (2000), pp. 3459–3480.
- [5] C CENEDESE AND C ADDUCE, *Mixing in a density-driven current flowing down a slope in a rotating fluid*, Journal of Fluid Mechanics, 604 (2008), pp. 369–388.
- [6] R H CLARKE, *Fair weather nocturnal inland wind surges and atmospheric bores: Part I Nocturnal wind surges*, Australian Meteorological Magazine, 31 (1983), pp. 133–45.
- [7] ———, *Colliding sea-breezes and the creation of internal atmospheric bore waves: two-dimensional numerical studies*, Australian Meteorological Magazine, 32 (1984), pp. 207–26.
- [8] N A CROOK, *Understanding Hector: The dynamics of island thunderstorms*, Monthly Weather Review, 129 (2001), pp. 1550–1563.
- [9] S T GILLE AND S G LLEWELLYN SMITH, *When land breezes collide: Converging diurnal winds over small bodies of water*, Quarterly Journal of the Royal Meteorological Society, (submitted).
- [10] S T GILLE, S G LLEWELLYN SMITH, AND S M LEE, *Measuring the sea breeze from quikSCAT scatterometry*, Geophysical Research Letters, 30 (2003), p. 1114.

- [11] M W MONCRIEFF AND C LIU, *Convection initiation by density currents: Role of convergence, shear, and dynamical organization*, Monthly Weather Review, 127 (1999), pp. 2455–2464.
- [12] H NIINO, *The linear theory of land and sea breeze circulation*, Journal of the Meteorological Society of Japan, 65 (1987), pp. 901–921.
- [13] J A NOONAN AND R K SMITH, *Sea-breeze circulations over Cape York Peninsula and the generation of Gulf of Carpentaria cloud line disturbances*, Journal of the Atmospheric Sciences, 43 (1986), pp. 1679–1693.
- [14] J R PACHECO, A PACHECO-VEGA, AND S PACHECO-VEGA, *Analysis of density currents using the non-staggered grid fractional step method*, in Proceedings of 5th International Symposium Stratified Flows, Citeseer, 2000, pp. 1135–1140.
- [15] R A PIELKE, *A three-dimensional numerical model of the sea breezes over south Florida*, Monthly Weather Review, 102 (1974), pp. 115–139.
- [16] J O SHIN, *Colliding gravity currents*, PhD thesis, University of Cambridge, 2001.
- [17] J O SHIN, S B DALZIEL, AND P F LINDEN, *Gravity currents produced by lock exchange*, Journal of Fluid Mechanics, 521 (2004), pp. 1–34.
- [18] J E SIMPSON, *Gravity currents in the environment and the laboratory*, Journal of Fluid Mechanics, 352 (1997), pp. 376–378.
- [19] J E SIMPSON AND P F LINDEN, *Frontogenesis in a fluid with horizontal density gradients*, Journal of Fluid Mechanics, 202 (1989), pp. 1–16.
- [20] J E SIMPSON, D A MANSFIELD, AND J R MILFORD, *Inland penetration of sea-breeze fronts*, Quarterly Journal of the Royal Meteorological Society, 103 (1977), pp. 47–76.
- [21] Z XIAN AND R A PIELKE, *The effects of width of landmasses on the development of sea breezes*, Journal of Applied Meteorology, 30 (1991), pp. 1280–1304.
- [22] H YAN AND R A ANTHES, *The effect of latitude on the sea breeze*, Monthly Weather Review, 115 (1987), pp. 936–956.

A Initial setup experiments

The table below provides details on the initial conditions for all experiments presented in this report.

Table 1: Initial conditions for all experiments. g'_1 and H_1 give respectively the value for reduced gravity (cm s^{-2}) and the lock height (cm) in the first lock, g'_2 and H_2 the same quantities for the second lock. Horizontal lines separate the full-depth, half-depth and partial-depth experiments.

	g'_1	H_1	g'_2	H_2	$\frac{g'_L}{g'_H}$	$\frac{g'H_1}{g'H_2}$
exp 01	9.0	20.0	8.8	20.0	0.99	1.01
exp 02	8.8	20.0	25.8	20.0	0.34	0.34
exp 03	9.7	20.0	11.3	20.0	0.86	0.86
exp 04	4.8	20.0	4.9	20.0	0.98	0.98
exp 05	5.1	20.0	9.6	20.0	0.53	0.53
exp 06	4.9	20.0	22.7	20.0	0.22	0.22
exp 07	4.8	20.0	19.4	20.0	0.25	0.25
exp 08	4.9	20.0	14.9	20.0	0.33	0.33
exp 09	14.1	20.0	18.9	20.0	0.74	0.74
exp 10	13.8	20.0	15.3	20.0	0.90	0.90
exp 11	18.5	20.0	23.5	20.0	0.79	0.79
exp 12	18.8	20.0	18.9	20.0	0.99	0.99
exp 13	9.4	20.0	15.3	20.0	0.61	0.61
exp 14	9.4	20.0	22.7	20.0	0.42	0.42
exp 15	9.7	20.0	20.3	20.0	0.48	0.48
exp 16	14.2	20.0	20.9	20.0	0.68	0.68
exp 17	4.9	20.0	7.1	20.0	0.69	0.69
exp 18	11.3	20.0	9.6	20.0	0.85	1.18
exp 19	4.9	20.0	5.2	10.0	0.94	1.88
exp 20	5.0	20.0	10.3	10.0	0.48	0.96
exp 21	9.7	20.0	5.2	10.0	0.54	3.90
exp 22	4.9	20.0	19.8	10.0	0.25	0.50
exp 23	9.5	20.0	10.0	10.0	0.95	1.90
exp 24	9.7	20.0	15.2	10.0	0.64	1.28
exp 25	9.9	20.0	21.0	10.0	0.47	0.94
exp 26	14.2	20.0	14.7	10.0	0.97	1.94
exp 27	15.0	20.0	20.1	10.0	0.75	1.49
exp 28	15.0	20.0	26.3	10.0	0.57	1.14
exp 29	9.8	20.0	24.8	10.0	0.40	0.79
exp 30	5.0	20.0	15.2	10.0	0.33	0.65
exp 31	4.7	20.0	24.3	10.0	0.19	0.39
exp 32	9.4	20.0	29.8	10.0	0.32	0.63
exp 33	5.2	20.0	20.9	5.0	0.25	0.99
exp 34	9.9	10.0	10.4	10.0	0.95	0.95
exp 35	5.0	20.0	13.5	7.5	0.37	0.99
exp 36	5.1	20.0	7.9	14.0	0.64	0.92